DANMARKS OG GRØNLANDS GEOLOGISKE UNDERSØGELSE RAPPORT 1997/1

Advanced Scanning Electron Microscope Analyses at GEUS

Karin Laursen

GEOLOGICAL SURVEY OF DENMARK AND GREENLAND
MINISTRY OF ENVIRONMENT AND ENERGY

GEUS

DANMARKS OG GRØNLANDS GEOLOGISKE UNDERSØGELSE RAPPORT 1997/1

Advanced Scanning Electron Microscope Analyses at GEUS

Karin Laursen

GEOLOGICAL SURVEY OF DENMARK AND GREENLAND
MINISTRY OF ENVIRONMENT AND ENERGY

GEUS

Table of contents

1. Introduction

For the last 15 years Scanning Electron Microscope (SEM) and Energy Dispersive X-ray (EDX) has been used extensively for solving problems related to coal combustion, especially in relation to the ash forming components of the coal: the minerals.

This report includes a description of the Scanning Electron Microscope at The Geological Survey of Denmark and Greenland (GEUS), and some of the analytical facilities connected to the microscope. Additionally, two techniques for performing automatical chemical analyses are described: Computer Controlled Scanning Electron Microscopy (CCSEM) and Scanning Electron Microscopy Point Counting (SEMPC). These two techniques were developed in connection with a project on slagging and fouling at GEUS for analyzing coal minerals, fly ashes and ash deposits. However both techniques can with minor changes be used for other materials, such as rocks, concrete, powders etc.

2. The Scanning Electron Microscope

This chapter includes an introduction to the Scanning Electron Microscope (SEM) at GEUS and the analytical facilities connected to the microscope. The literature used in this chapter includes: Goldstein et al, 1992; Southworth, 1975; and notes from a basic SEM course by Phillips;

2.1. Scanning Electron Microscope

The scanning electron microscope at GEUS is a Philips XL 40, equipped with a NORAN Instruments Voyager 1100 microanalysis system with digital imaging.

A scanning electron microscope uses an electron beam as an image source. Figure 2.1. contains a sketch of the main component of a SEM. The electron beam originates in the electron gun formed by a tungsten filament (1). A tungsten filament is a bent V-shaped wire (100 μm diameter) that is heated resistively by a filament heater power and held at a high negative potential by a high voltage supply (Figure 2.2). At the operating temperature, electrons are emitted from the filament in all directions.

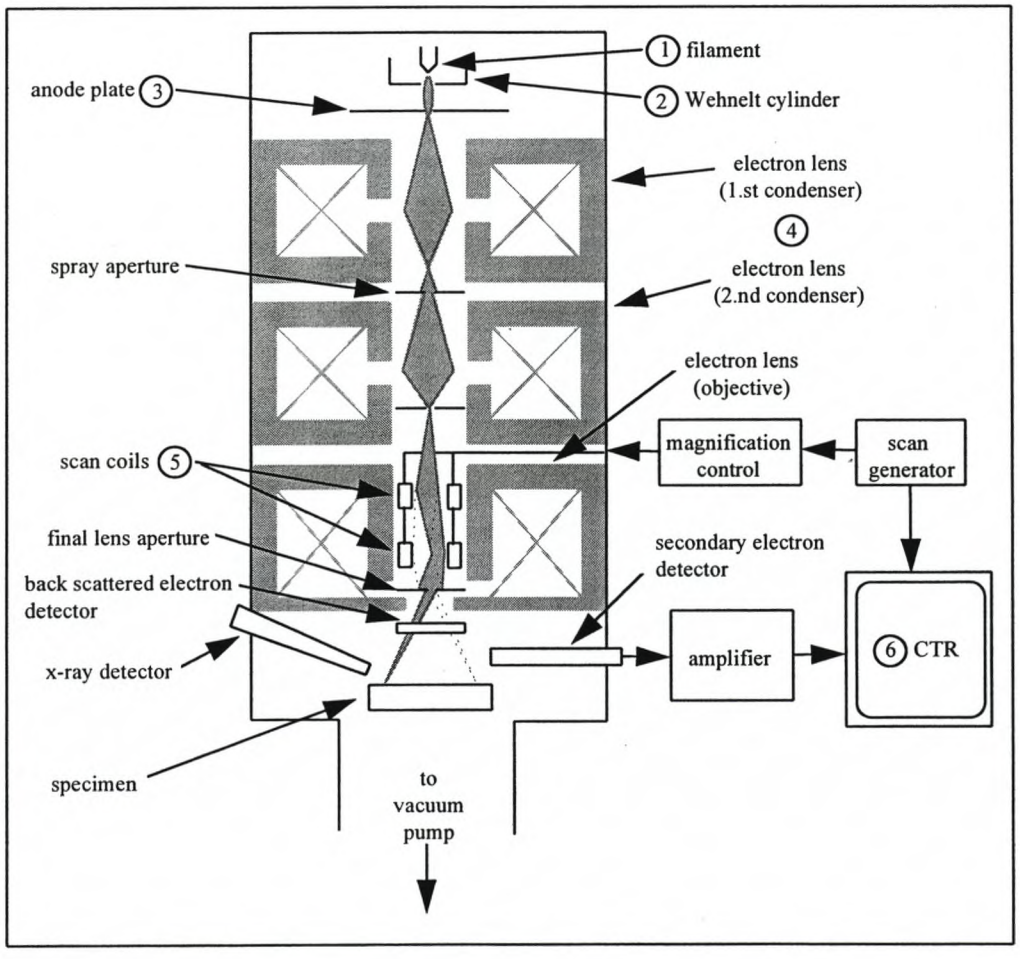

Figure 2.1. Schematic drawing of a scanning electron microscope. The numbers on the figure refer to explanations in the text (modified after Goldstein et. al., 1992).

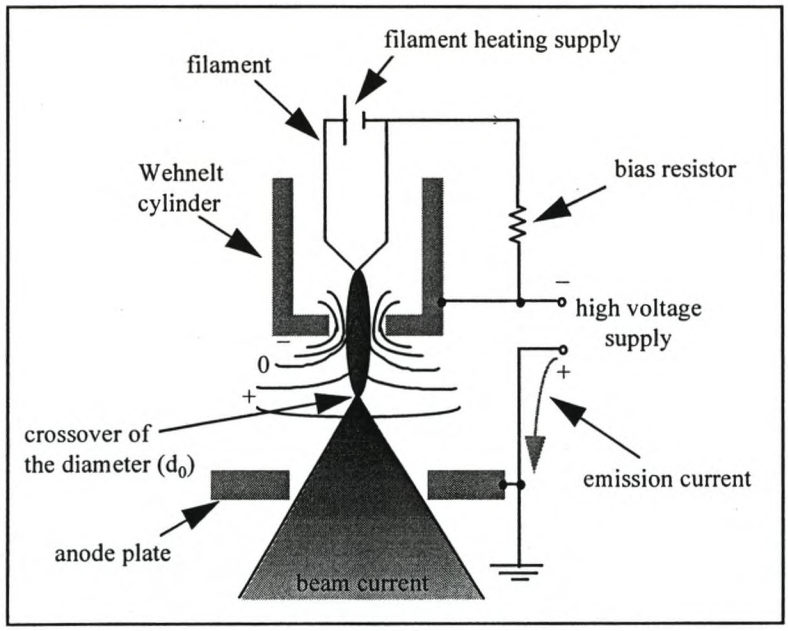

Figure 2.2. Schematic drawing of a self-biased thermo-ionic electron gun (modified after Goldstein et. al., 1992).

To achieve a good image and precise microanalyses is it essential that the beam current is constant. A stable beam current requires a condition of filament saturation, that is a condition where a small increase in the filament current no longer leads to an increase in the beam current.

A grid cap (Wehnelt cylinder (2) and Figure 2.2) focuses the electrons inside the gun and controls the amount of electron emission. The Wehnelt cylinder is maintained at a slightly more negative potential than the filament itself, using a variable bias resistor as a voltage divider that provides a bias voltage on the grid cap. This bias voltage varies with the emission current and gives rise to the term "self-biased electron gun".

An anode plate (3), placed below the Wehnelt cylinder (Figure 2.2), acts as an accelerator to accelerate the electrons from the high negative potential at the filament (acceleration voltage: -1 to -30 kV) to ground potential (0 V) at the anode. A hole (aperture) in the anode allows a small a fraction of the emitted electrons to continue as the beam current down through the column towards the lenses (4). Electrons collected on the anode (emission current) return to the ground to the high voltage power supply. The beam current is often characterized by the current density (current / area) so that the relative intensity of the beam may be measured at any point in the column, regardless of the fraction of the beam sampled.

Electron lenses (4) (electromagnetic) are used to demagnify the crossover in the electron gun (10-50 μm) to a final spot size on the specimen (1nm-1μm) (Figure 2.2). SEMs employ one to three condenser lenses to demagnify the electron beam cross-over diameter. The first condenser lens controls the demagnification. The more current flowing through the condenser, the smaller the size of the final probe and the smaller the beam current that reaches the specimen. The final lens in the column is

called the probe forming or objective lens, and it acts to focus the image by controlling the movement of the probe cross-over along the optic axis of the column.

To produce an image of the specimen the signal intensity from the beam-specimen interactions are measured point by point across the surface of the specimen. The beam scans along a line across the specimen and then parallel displaces the line position a little to start a new scan. The scanning over the surface is controlled by two electromagnetic deflection coils (scan coils (5)) placed inside the objective lens. The magnification of the specimen image is the ratio of the linear size of the viewing screen (cathode ray tube, CRT (6)) to the length of the scan.

During operation the electron beam is scanned over the surface of the specimen where it interacts with the near surface (to a depth of approximately 1 μm) and generates signals used to form images or to perform chemical microanalyses.

Electrons entering the specimen surface will respond to the atoms of the specimen. When an electron passes close to an atom the presence of the atomic and nuclear potential will disturb (scatter) the initial velocity of the electron (Figure 2.3). The velocity change may be only directional (elastic scattering) or both direction and the kinetic energy of the electron may be changed (inelastic scattering). Elastic scattering is responsible for the phenomenon of Electron Back Scattering (BSE). Inelastic scattering events of several types result in transfer of energy from the beam electrons to the atoms of the specimen leading to the generation of Secondary Electrons (SE), Auger electrons and characteristic x-rays.

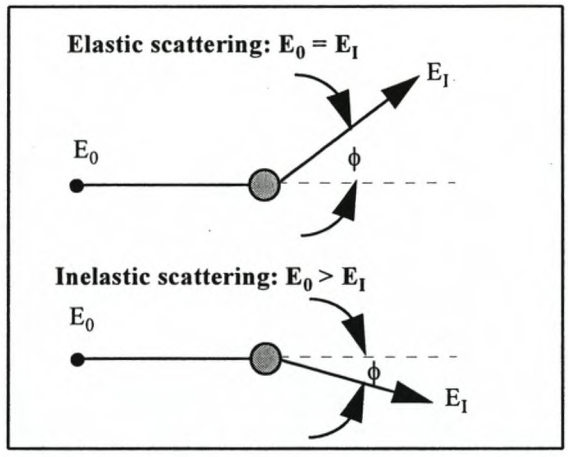

Figure 2.3. Scattering of electrons by atoms in a specimen. Elastic scattering leads to a conservation of the kinetic energy of incoming electron (E_0), whereas inelastic scattering leads to a loss of energy from the electron to the atom ($E_0 > E_I$). The scattering angle (ϕ) is much higher for elastic scattering than for inelastic scattering (modified after Goldstein et. al., 1992).

If an electron penetrates into the nucleus of an atom the positively charged nucleus has a large influence on the velocity of the electron but there is a conservation of energy and momentum, thus, this is an elastic scattering process. An electron entering the specimen will also interact with the electron cloud around the nucleus of the atoms, mainly resulting in: 1) inelastic scattering of the electron and 2) transfer of its energy to the atom. As a result of this interaction, electrons in atomic shells will be

released and / or excited. Due to the relatively lower energy required to remove electrons from the outer shells, mainly outer shell electrons are involved. The released electrons drift through the material and are subjected to the inelastic scattering processes as well. The drifting electrons have a low energy and they can only escape from the material if they are close to the surface. These electrons are known as Secondary Electrons (SE).

The electron scattering process in a specimen is a random event, and by using both elastic and inelastic multiple scattering models and probabilities for scattering angles and energy transfer in a Monte Carlo simulation, the scattering pattern of electrons in various materials may be calculated.

The penetration depth of the electrons depends on the material composition that influences both the elastic and the inelastic scattering processes. The inelastic scattering, resulting in slowing down of the electrons is far more efficient for high Z materials (high atomic number) than for low Z materials. This means that although the elastic scattering increases for high Z materials the penetration is smaller than for low Z materials. This increased elastic scattering for high Z material is important for the Back Scattered Electron (BSE) image.

The two most common signals used for producing images are Secondary Electrons (SE) and Back Scattered Electrons (BSE), and the signals used for performing chemical analyses are x-rays.

Secondary electrons (SE)

Electrons that are emitted from the specimen with an energy less than 50 eV are defined as Secondary Electrons (SE). Ionization of atoms occurs and electrons are released throughout the total interaction volume, but only the secondary electrons generated close to the surface will leave the specimen and contribute to the signal. The contributing depth is about 1 nm for metals and in the order of 10 nm for carbon.

Back Scattered Electrons (see later) generated deep in the material posses energy enough to produce secondary electrons on their way back to the surface (Figure 2.4). This means that SE is also generated outside the actual interaction of the primary electron beam. However, the number of these SE is small compared to the primary ones and can be ignored.

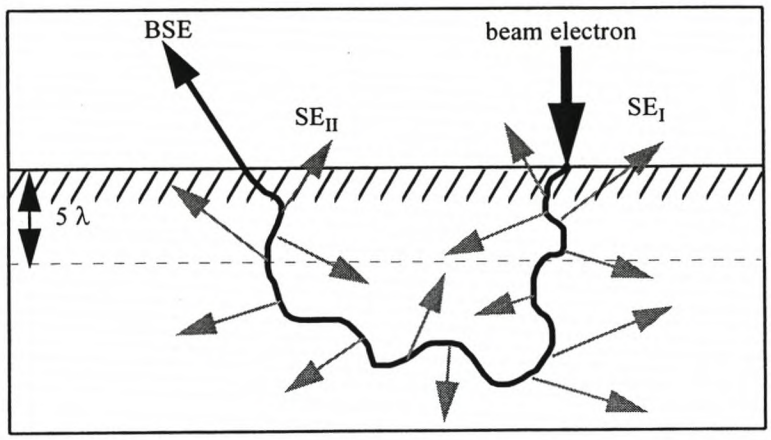

Figure 2.4. Illustration of the origin of two sources of secondary electrons in a sample. Incident beam electrons generate secondary electrons (SE_I) and back scattered electrons generate secondary electrons (SE_{II}) while leaving the sample. λ is the mean free path for secondary electrons (modified after Goldstein et. al., 1992).

The Secondary Electrons are collected by an Everhart-Thornley (E-T) electron detector located at the side of the chamber (Figure 2.5). The E-T detector consists of a scintillator, a light pipe and a photomultiplier tube. The detector is electrically isolated from the rest of the microscope and has a wire mesh screen (grid) in front of it with a potential of about +300 V to attract the low energy secondary electrons into the detector from anywhere in the specimen chamber. When the electrons pass through the grid they will be affected by a +10 kV potential from a thin aluminum coating on the surface of a high scintillator material. This high potential is applied to give the electrons sufficient energy to produce photons of light when they strike a scintillator. These photons of light pass down a light pipe to an optical window and are picked up by a photomultiplier mounted outside the chamber.

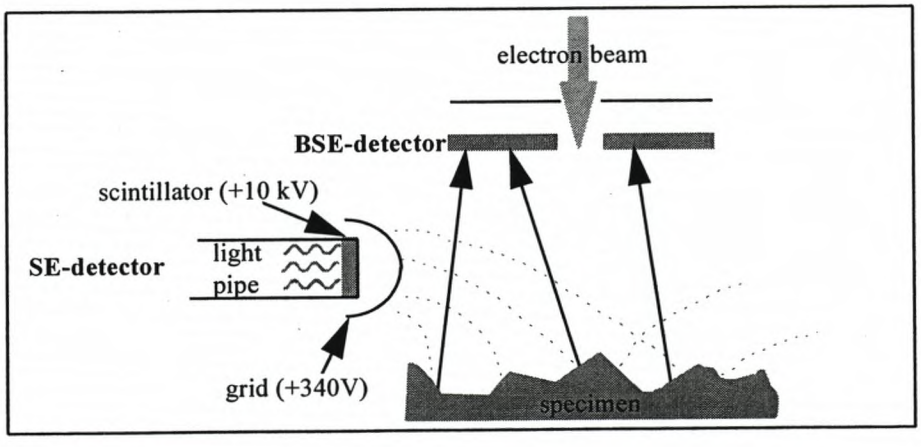

Figure 2.5. Electron collection by SE and BSE detectors from randomly oriented surfaces (modified after Goldstein et. al., 1992).

The image produced from secondary electrons is a light / shadow image reflecting the surface of the specimen (Figure 2.6). A larger percentage of secondary electrons produced on surfaces pointing towards the detector will be attracted to the potential of

the wire mesh, thus these surfaces will be relatively more bright than surfaces pointing away from the detector (Figure 2.6).

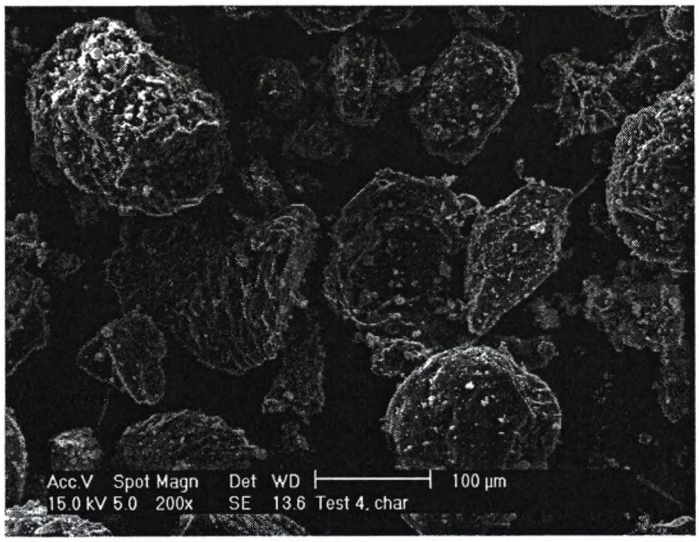

Figure 2.6. Secondary electron image of char particles. The sides of the particles faced towards the upper left corner is brighter than any other sides, due to the detector located by the upper left corner.

Back scattered electrons (BSE)

The Back Scattered Electrons are the result of electrons from the primary beam undergoing a sequence of elastic and inelastic scattering events, in which the net change in direction is sufficient to carry them out of the specimen. The BS electrons are the electrons with energies higher than 50 eV. As a result of elastic interaction the electron may become a back scattered electron with a maximum energy equal to the primary electron energy.

Strictly speaking back scattering refers to a single elastic scattering event in which the electron trajectory is changed by more than 90^{o} from the forward direction of motion, so that the scattered electrons propagate back into the hemisphere of the original electron beam. However, the back scattered electrons escaping from the surface of the specimen can be the result of numerous elastic scattering events within the sample.

In practice, the E-T detector may also be used for collecting back scattered electrons, but the SEM at GEUS is equipped with a separate BSE electron detector of the solid-state diode type. A solid-state diode detector is based on a semiconductor (Sears et. al, 1982; Mortimer, 1983), in which electron hole-pairs are produced by the incoming high energetic back scattered electrons. The electron-hole production in the solid-state diode detector serves to increase the signal from the specimen by about three orders of magnitude.

BS-electrons are very useful for creating images in a SEM, because the back scattered electrons respond to the composition of the specimen. Due to the earlier mentioned effect of increasing elastic scattering for high atom number materials, the number of back scattered electrons increase with increasing atom number. Thus, a Back

Scattered Electron image reflects the contrast in the composition of the specimen surface (Figure 2.7).

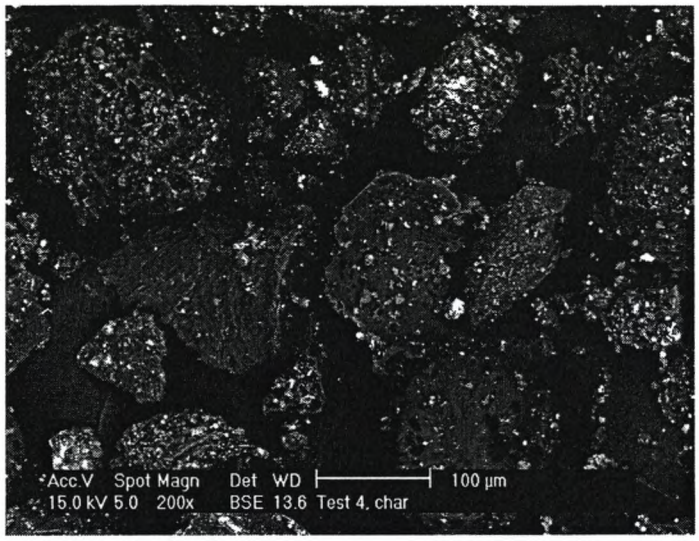

Figure 2.7. Back scattered electron image of the same chars illustrated on the secondary electron image in Figure 2.6. The small spherical fly ash particles (mainly Al-silicates) consist of a material with a higher average atom number, than the organic chars (mainly C), thus the fly ash particles will appear much brighter than the char particles.

Microanalysis (X-ray)

When a beam electron interaction result in ionization of an atom, the atom is left with a vacancy in one of its shells. One way for the atom to fill the vacancy is to catch one of the electrons of a higher shell. When an electron in the shells close to the nucleus jumps from a higher to a lower shell the differences in energy will be emitted as an x-ray quantum (Figure 2.8). Since the electron energy levels of an atom are fixed, and since the allowed jumps from one shell to another are subjected to strong quantum mechanical selection rules, the energy and the wavelength of the emitted x-ray quantum is characteristic for the atom itself. Another way for the atom to loose the excess of energy is that the emitted x-ray ejects an electron of another shell, thus resulting in the generation of an electron with an energy characteristic for the material. These electrons have an energy of up to about 2 keV, and are called Auger electrons.

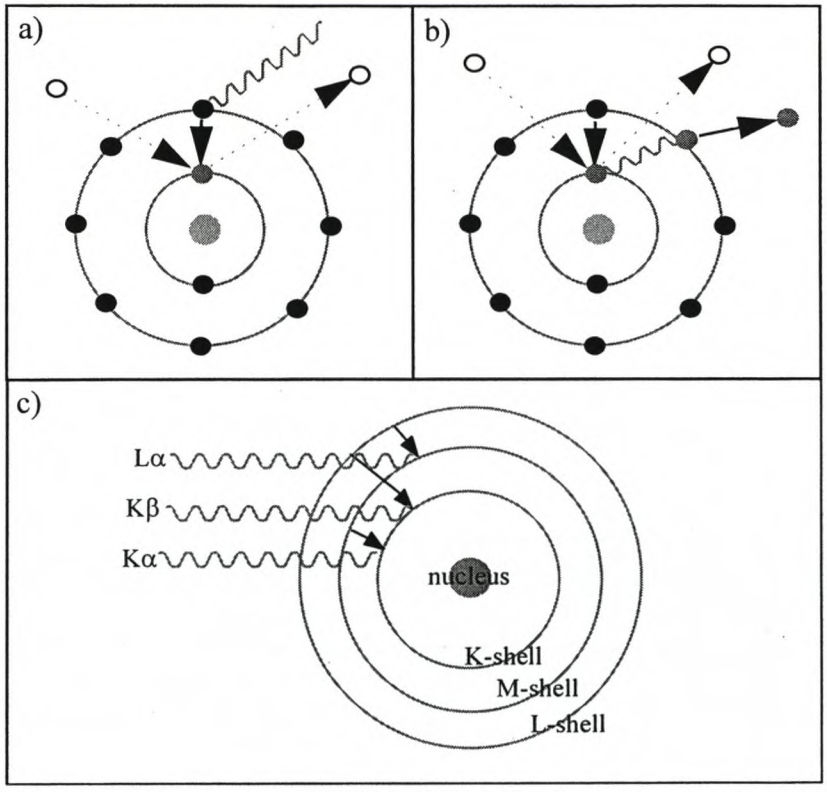

Figure 2.8. Schematic illustration of emission of **a)** x-ray emission, **b)** Auger electrons and **c)** characteristic Kα, Kβ and Lα x-ray.

The emitted x-ray quantum possess atom characteristic energies and wavelength that may be used for performing microanalysis. The detection of the x-ray can either be made by and Energy-Dispersive System (EDS) or Wavelength-Dispersive System (WDS). If a SEM is equipped with only one detector system, usually this would be an EDS, but for trace element analyses it is generally necessary to operate with WDS, which has a much higher resolution than EDS systems. Thus more and more systems are retrofitted with WDS. The SEM at GEUS is only equipped with an EDS system.

In the energy-dispersive system, the active detector medium is a Si(Li) crystal which converts the x-ray quantum to an electrical pulse, with a charge proportional to the energy of the detected x-ray photons. A qualitative x-ray analysis of a specimen involves the identification of the elements present in the specimen by determining the energies of the characteristic radiation generated from the sample. An energy-dispersive x-ray spectrum illustrates the energy (keV) versus the number of counts of photons (Figure 2.9). Based on the specific energies of the x-ray quantum for different electron jumps it is possible to identify all the peaks within a spectrum, providing a qualitative analysis. The information needed to identify the peaks of the spectrum are normally incorporated in the computer software associated with the analytical system and the identification can be done automatically.

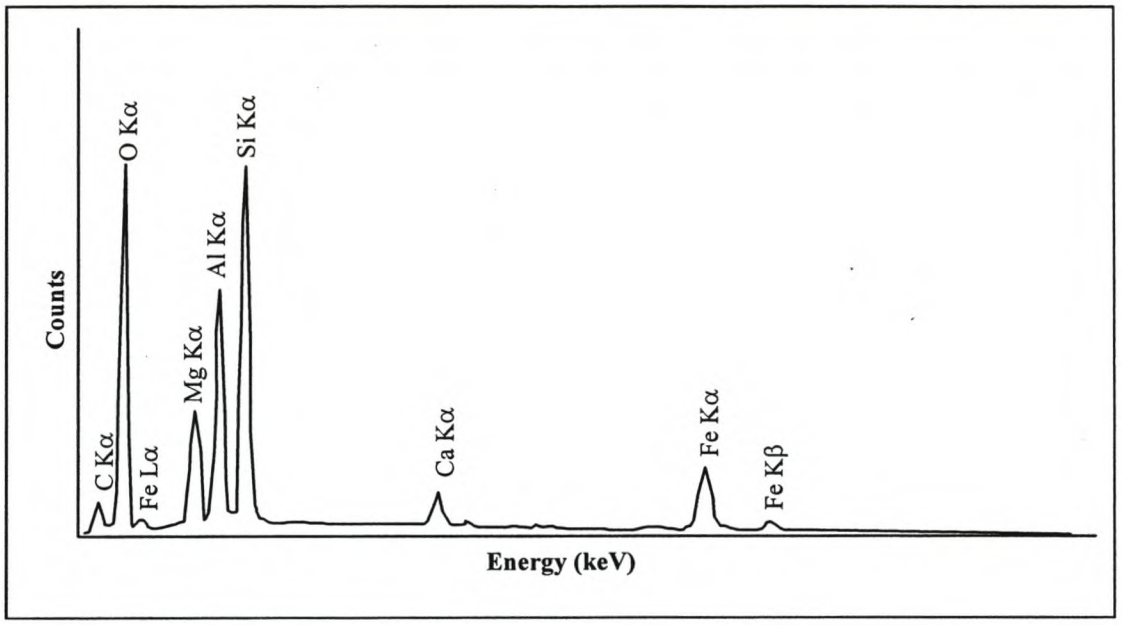

Figure 2.9. EDX spectrum for chlorite $((Mg,Al,Fe,)_{12}((Si,Al)_8O_{20})(OH)_{16})$ shows the intensity of the characteristic x-ray for each element present in the analyzed particle. The C Kα peak originates from the carbon coating of the specimen. Specimens has to be coated with a thin conductive layer (carbon or gold) to avoid charging from the electron beam.

The energy dispersive x-ray spectrum also makes it possible to determine the chemical composition of a specimen quantitatively, with an output given in atom percentage, element weight percentage or oxide weight percentage. Basically, the quantification of an EDX analysis involves measuring the peak intensity for a given energy and relating the intensity to the intensity in a standard of known composition. Thus, it would seem simple to perform a quantitative analysis: first compare the characteristic x-ray intensity measured on the specimen to that measured on the standard and that ratio would be equivalent to the ratio of concentration of the element in the specimen compared to that of the standard. However, the quantification needs to be corrected for various errors inherent in the measurement, due to differences in the behavior of the electrons and photons within the unknown specimen and the standard. These effects are known as matrix- or inter element effects, and arise because of differences in elastic and inelastic scattering processes as well as the propagation of x-rays through the specimen to reach the detector. The matrix effects are generally divided into three components: those due to atomic number (Z), x-ray absorption (A) and x-ray fluorescence (F), in total called a ZAF-correction.

The effects of *atomic number* arise from the electron back scattering and the electron retardation, both of which depend on the atomic number of the sample. Thus, if there is a significant difference in the composition of the specimen and the standard, an atomic number correction is required. In general, unless this effect is corrected, analyses of heavy elements in a light matrix generally yield concentrations which are too low, while analysis of light elements in a heavy element matrix usually yield concentrations that are too high.

To reach the detector the emitted x-rays pass through the specimen and photoelectric *absorption* from interactions with the atoms of the specimen will decrease the intensity. However, it is important to underline that the x-ray photons either are absorbed or pass through the specimen with their original energy, so that any photon that reaches the detector will still have an energy characteristic of the atom that emitted it. Absorption follows an exponential law, which means that as x-rays are generated deeper in the specimen a progressively greater fraction is lost to absorption. The absorption is dependent on three variables: the operating voltage, direction of the x-ray (take off angle), and the mass absorption coefficient for the element in the specimen. X-ray absorption is usually the most important factor that must be considered in measurements of compositions by x-ray microanalysis.

Photoelectric absorption results in the ionization of inner atomic shells, and those ionization's can also cause emission of characteristic x-rays. For *fluorescence* to occur, the target must contain species of atom with a critical excitation energy less than the energy of the characteristic x-rays being absorbed. In such a case, the measured x-ray intensity from this second element will include both the direct electron-exited intensity and the additional intensity generated by the fluorescence effect. Generally, the fluorescence effect can be ignored unless the photon energy exceeds the edge of the energy by less the 5 keV. The fluorescence factor is usually the least important in the ZAF correction.

ZAF correction of x-ray microanalysis can in most SEM systems be carried out in two ways, either by using internal standards which are standards included in the system by the manufacturer (usually called standardless analysis) or by using operator included standards, in which standards are analyzed by the operator prior to analyzing the unknown standard.

In practice a ZAF correction is performed by first comparing the intensity of each element in the specimen with the intensity of the standards, these values are called k-values and are proportional to the concentration of a given element. These measured k-values are used as the first estimate on the composition, and are normalized to sum to 100%. These initial mass fractions are used to compute the initial ZAF factors for each element. The estimated concentrations and ZAF factors for each element are used to calculate new k values that are then compared to the measured k-values. In this way iterations proceeds until the results converge.

The surface of the specimen is another important factor has to be considered when performing microanalyses. To achieve a good result of an x-ray analysis it is important that the specimen surface is planar and smooth, since even small irregularities may have influence on the result.

Major advantages of x-ray microanalysis in the SEM is that the analysis is obtained from a small volume and that the technique is nondestructive. However the main strength of the system lies in the combination of visual observations (SE-, BSE images) of the specimen (i.e. morphology, texture) with chemical analysis.

3. Computer Controlled Scanning Electron Microscopy (CCSEM)

The CCSEM technique is used to determine the size, shape, quantity, and semi-quantitative composition of particles. The technique may be used on any material where a phase can be distinguished by its color or shape from the rest of the sample either on a BSE or SE image. The technique was mainly developed for investigation of minerals in coal and fly ash particles (Lee et al., 1978, Huggins et al., 1980; Zygardlicke & Steadman, 1990; Jones et al., 1992). However, the technique can easily be applied on other materials such as powders, cement or rock minerals. The method and its applications in coal and mineral research were reviewed recently by Skorupska and Carpenter (1993). The components in the SEM system used in the CCSEM technique include: the Back Scattered Electron (BSE) detector, the stage control, the beam control, and the Energy Dispersive X-ray (EDX) detector.

3.1. Analytical procedure

The specimen to be analyzed is first embedded in a mounting material. For most samples epoxy may be used, but for coal carnauba wax is used since it provides a better BSE distinction from the coal particles than epoxy. Approximately 2 grams of specimen is used. The mounted sample is then grinded and polished with 1 μm and 1/4 μm diamond paste. To prevent dissolution of water soluble minerals and salts during sample preparation, lapping oil is used for cutting the samples and isooctane or an alkan mixture for polishing. The prepared sample is then cleaned with isooctane and carbon coated.

On the sample, the uppermost left and the lowermost right positions are located and the stage control is set to select multiple randomly distributed fields between the two corner positions. In order to give an equal statistical representation of large and small particles in the analysis, each located field is analyzed at three magnifications: 25x, 100x, and 500x. For each magnification only a defined particle size range is analyzed: 25x ([1 μm; 4 μm[ ), 100x ([4 μm; 32 μm[ ), 500x ([32 μm; 250 μm[ ). A Back Scattered Electron (BSE) image is acquired on each field. As the BSE intensity is a function of the average atomic number of the surface of the sample the higher atomic number minerals appear brighter than the lower atomic number coal particles and the lowest atomic number carnauba wax appears black (Figure 3.1). The BSE image is a digital image consisting of 512 x 512 image points (pixels). Each pixel in the image possesses a grey level value between 0 and 255, which is related to the brightness of the point. The grey level value of black is 0 and the value of white is 255.

Figure 3.1. Back scattered electron image (digital image, 512 x 512 pixels) of a carnauba wax embedded pulverized coal sample. The minerals appear white, the coal particles are grey and the carnauba wax is black.

Figure 3.2 illustrates a histogram over brightness levels on the BSE image shown in Figure 3.1. The grey level intensity from black to white is shown on the abscissa of the histogram. The ordinate shows the area proportion of each grey level intensity. The histogram may be used for estimating the area percentage of coal and mineral matter in a coal sample. Based on the grey levels, a threshold value for the minerals can be set. The analytical system will identify any particle with a grey level higher than this threshold as a mineral.

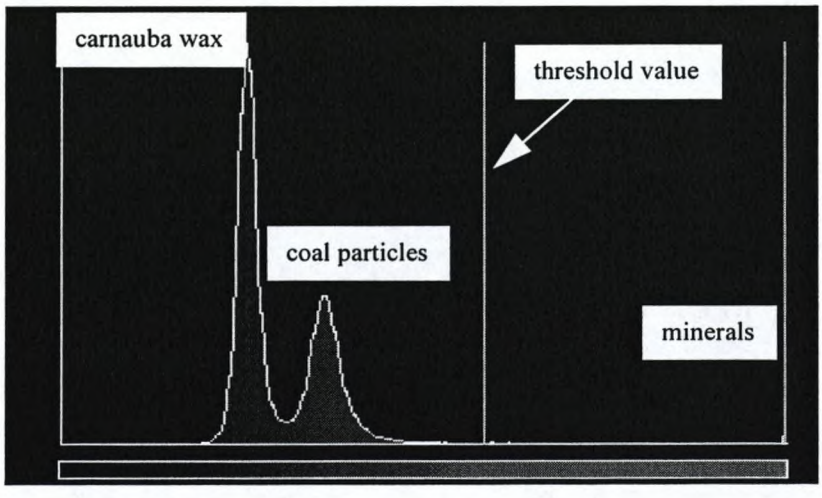

Figure 3.2. Distributions of brightness levels in the BSE image shown in Figure 3.1. From left to right the two peaks represent carnauba wax (black) and the coal particles (grey). The minerals are represented by the area from the threshold value to the small peak by the white end of the intensity level.

A binary digital image (512 x 512 pixels), with the minerals as the white component and coal particles + carnauba as the black component, is created by use of the threshold value (Figure 3.3).

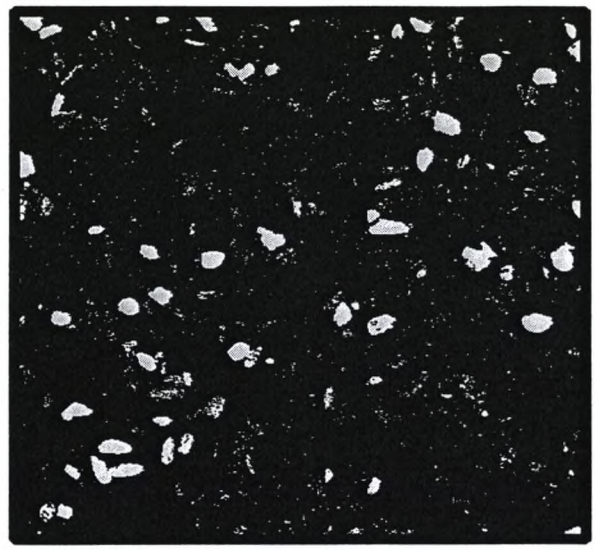

Figure 3.3. Binary image created based on the threshold value shown in Figure 3.2.

The binary image is used by the scanning electron microscope to automatically locate and determe the size and shape of each mineral particle. The size of a pixel is dependent on the magnification. The area of the pixels at the 3 magnifications used for CCSEM analyses are: 25x (49.27 μm^2), 100x (3.079 μm^2) and 500x (0.1232 μm^2). Adhering white pixels constitute one particle and the size and shape of each particle is determined by the number of pixels in each particle and their internal distribution. Based on these data a sizing image is created (Figure 3.4).

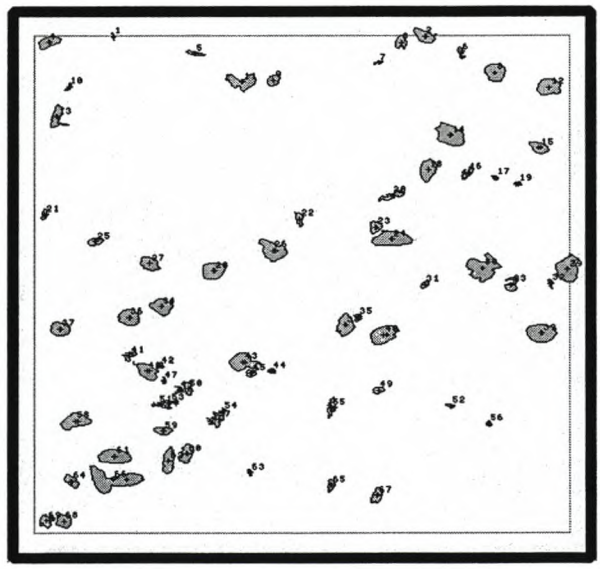

Figure 3.4. Sizing image of the image shown in Figure 3.1 and Figure 3.3. The numbers on the particles refer to the number of the particle within the frame.

The beam control unit is set to scan each particle and collect an EDX spectrum for 5 seconds. An EDX spectrum shows the intensity of the characteristic x-ray for each element present in the analyzed particle (Figure 3.5).

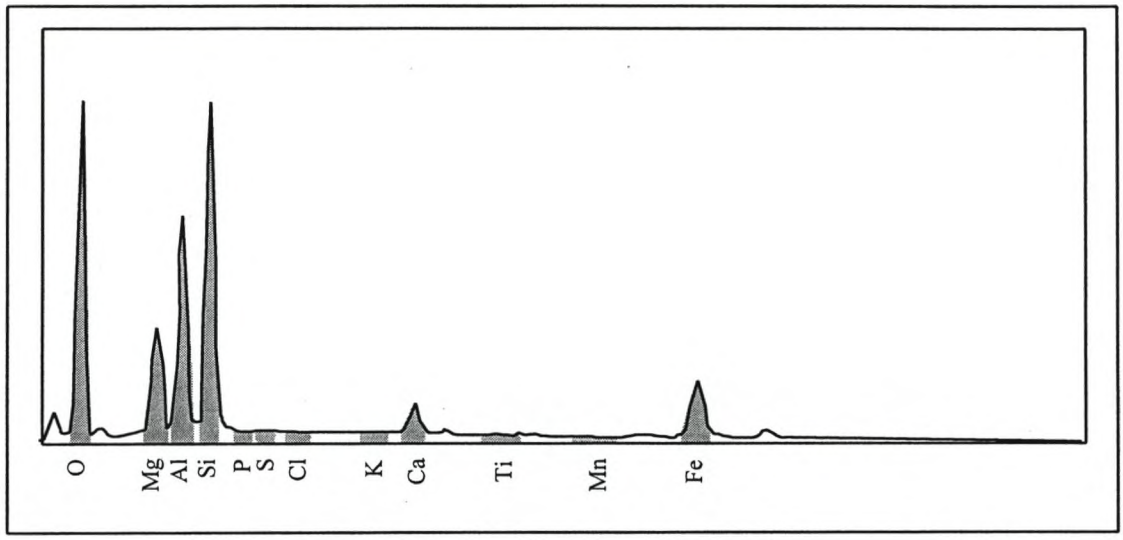

Figure 3.5. EDX spectrum for chlorite shows the intensity of the characteristic x-ray for each element present in the analyzed particle. The Regions Of Interest (ROI) are indicated by the grey colored areas on the spectrum.

Based on knowledge of the characteristic x-ray energies for each element, corresponding energy regions are created for each element (Regions Of Interest, ROI)(Figure 3.5). All counts detected within the ROI for each element will be assigned to that element. The x-ray spectrum is processed to determine the apparent concentration of 15 elements (O, Na, Mg, Al, Si, P, S, Cl, K, Ca, Ti, Cr, Fe, Ni, Cu). The concentration of each element is determined by dividing the counts within the Region Of Interest for each of the elements with the total amount of counts within all 15 ROI. The concentration of each element determined by this type of analysis is given in percent of total counts, whereas the normal output from traditional Energy Dispersive X-ray analysis is given either in atomic percent or element weight percentage. For further handling of the data the percentages of counts are set to be equivalent to element weight percentage. The assumption that the output should be equal to element weight percentage is a major approximation, and can only be justified since the chemical composition mainly is used to group the data into chemical categories . Due to the way the composition of the particles is determined it is not possible to perform ZAF corrections on the analyses to account for the effects of atomic number (Z), absorption (A) and fluorescence (F).

The output from a CCSEM analysis is collected on-line by a computer, and consists of a data file (Table 3.1). The output file contains the frame number, the particle number within the frame, cumulative particle number, total number of counts, particle area (based on pixels) and the chemical composition of the particle (percent of counts). A normal CCSEM analysis contains data on a total of 2000-5000 particles from 10-20 frames at each magnification. The number of frames and number of particles analyzed depend on the concentration of minerals in the individual coal sample.

frame	particle	cum.	area	counts	O	Na	Mg	Al	Si	P	S	Cl	K	Ca	Ti	Fe	Ni	Cu	Cr
1	1	1	1380	6729	23	0	0	0	0	0	0	0	0	77	0	0	0	0	0
1	2	2	1971	10875	25	0	0	0	75	0	0	0	0	0	0	0	0	0	0
1	3	3	2020	8947	26	0	0	32	42	0	0	0	0	0	0	0	0	0	0
1	4	4	1232	8690	25	0	0	28	46	0	0	0	0	0	0	0	0	0	0
1	5	5	1084	2072	54	0	17	0	0	0	0	3	0	0	0	26	0	0	0
1	6	6	1133	1735	42	53	0	4	0	0	0	0	0	0	0	0	0	0	0
1	7	7	1725	10427	24	0	0	30	46	0	0	0	0	0	0	0	0	0	0
1	8	8	1872	7251	25	0	0	30	45	0	0	0	0	0	0	0	0	0	0
1	9	9	1133	3184	44	49	0	0	0	0	7	0	0	0	0	0	0	0	0
1	10	10	985	6199	26	0	15	12	23	0	0	0	3	21	0	0	0	0	0
2	1	11	1330	6039	24	0	0	0	0	0	0	0	0	76	0	0	0	0	0
2	2	12	1971	10943	27	0	0	0	73	0	0	0	0	0	0	0	0	0	0
2	3	13	1527	7910	24	0	0	31	41	0	0	0	4	0	0	0	0	0	0
2	4	14	1380	7902	24	0	0	28	48	0	0	0	0	0	0	0	0	0	0
2	5	15	1035	2422	47	0	15	0	4	0	0	0	0	6	0	27	0	0	0
2	6	16	1478	8734	25	0	0	28	47	0	0	0	0	0	0	0	0	0	0
2	7	17	2168	5664	22	0	0	27	51	0	0	0	0	0	0	0	0	0	0
2	8	18	1133	3003	43	49	0	0	4	0	0	0	0	0	4	0	0	0	0
2	9	19	985	5486	25	0	14	14	27	0	0	0	0	19	0	0	0	0	0
2	10	20	1626	5025	24	0	0	33	43	0	0	0	0	0	0	0	0	0	0
3	1	21	8327	5433	65	0	0	0	0	0	0	0	0	0	0	35	0	0	0
3	2	22	1281	9736	23	0	0	29	44	0	0	0	4	0	0	0	0	0	0
3	3	23	2858	9802	23	0	0	21	56	0	0	0	0	0	0	0	0	0	0
3	4	24	4336	6726	26	0	0	42	14	12	0	0	0	5	0	0	0	0	0

Table 3.1. Raw data file from CCSEM analyses of a coal.

Comparisons between the Back Scattered Electron Image (Figure 3.1) and the sizing image (Figure 3.4) may be used to evaluate if a mineral is located inside a coal particle (inherent or included) or as an independent particle (extraneous or excluded). So far the included/excluded evaluation is carried out manually at GEUS, but it is planned to automate this procedure in the future.

3.2. Data reduction

The chemical composition of each particle is used to classify the particles into one of 33 mineral or chemical categories (Table 3.2). The category system used at GEUS is developed on the bases of the system used at the Energy and Environmental Research Center, University of North Dakota (Zygardlicke & Steadman, 1990; Jones et al., 1992). As can be seen in Table 3.2 the categories are mixtures of mineral names and "chemical composition groups". The counts from oxygen are included in the ROI, but it is not implemented into the categories, due to the analytical problems with analyzing light elements.

quartz: Al <= 10, Si >= 80
iron oxide: Mg <= 5, Al <= 5, Si < 10,S <= 5, Fe >= 80
periclase: Mg >= 80, Ca <=5
rutile: S <= 10, Ti >= 80
alumina: Al >= 80
calcite: Mg <= 5, Al <= 5, Si <= 5, P <= 5, S < 10, Ca >= 80, Ti <= 5
dolomite: Mg > 5, Ca > 10, Mg + Ca >= 80
ankerite: Mg < Fe, S < 15, Ca > 20, Fe > 20, Ca + Mg + Fe > 80
kaolinite: Na <= 5, K <= 5, Ca <= 5, Fe <= 5, Al + Si > 80, (0.8 * Al) < Si, Si < (1.5 * Al)
montmorillonite: Na <= 5, K <= 5, Ca <= 5, Fe <= 5, Al + Si > 80, (1.5 * Al) < Si, Si < (2.5 * Al)
illite: Na <= 5, Al >= 15, Si > 20, K > 5, K + Al + Si >= 80, Ca <= 5, Fe <= 5
Fe-Al silicate: Na <= 5, Al >= 15, Si > 20, S <= 5, K <= 5, Ca <= 5, Fe > 5, Fe + Al + Si >=
Ca-Al silicate: Na <= 5, Al >= 15, Si > 20, S <= 5, K <= 5, Ca >= 5, Ca + Al + Si >= 80, Fe <= 5
Na-Al silicate: Na >= 5, Al >= 15, Si > 20, Na + Al + Si >= 80, S <= 5, K <= 5, Ca <= 5, Fe <= 5
aluminosilicate: Na <= 5, Al > 20, Si > 20, Si + Al >= 80, K <= 5, Ca <= 5, Fe <= 5
mixed silicate: Na < 10, Al > 20, Si > 20, S <= 5, K < 10, Ca < 10, Fe < 10, Na+Al+ Si+K+Ca+F >80
Fe silicate: Na <= 5, Al <= 5, Si < 20, S <= 5, K <= 5, Ca <= 5, Fe > 10, Fe + Si >= 80
Ca silicate: Na <= 5, Al <= 5, Si > 20, S <= 5, K <= 5, Ca > 10, Ca + Si >= 80, Fe <= 5
Ca aluminate: Al > 15, Si <= 5, P <= 5, S <= 5, Ca > 20, Ca+Al >= 80
pyrite: S > 40, Ca < 10, Fe >= 10, Fe + S >= 80, Fe <= (S * 0.7)
pyrrhotite: Fe + S >= 80, Fe > 20, S > 20, (0.7 * S) < Fe, Fe < (1.5 * S), Ca < 10
oxi. pyrrhotite: Fe + S >= 80, Fe > 40, S > 5, Fe >= (1.5 * S), Ca < 10
quartz-pyrite: Al < 5, Si > 10, S > 10, Fe > 5, Fe <= (S * 0.7), Si+S+Fe > 80, Na < 5,K < 5, Ca < 5
clay-pyrite: Al > 5, Si > 10, S > 10, Fe > 5, Fe < =(S * 0.7), Si+S+Fe > 80, (0.6*Al) < Si, Al < (2.6 Si)
Fe-Cr oxide: Fe + Cr > 70, Fe > 35, S < 15
Cr-Fe oxide: Fe + Cr > 70, Fe < 35, S < 15
gypsum: Si < 10, S > 20, Ca > 20, Ca + S > 80, Ti < 10
apatite: Al <= 5, P >= 20, S <= 5, Ca >= 20, Ca + P >= 80
Ca-Al-P: Al > 10, Si <= 5, P > 10, S <= 5, Ca > 10, Al + P + Ca >= 80
KCl: K >= 30, Cl >= 30, K + Cl >= 80
gypsum/rutile: S > 20, Ca > 5, Ti > 5, Fe <= 5, S+Ca+Ti >= 80
gypsum/Al silicate: Al > 5, Si > 5, S > 5, Ca > 5, Al + Si + S + Ca >= 80
Si-rich: Si >= 80
Ca-rich: Ca >= 80
Ca-Si-rich: Si >= 20, Ca >= 20, Si + Ca >= 80
unknown: all non-categorized

Table 3.2. Chemical classification system for CCSEM data.

It is apparent from the list of categories and their compositions, that a category with a mineral name (e.g. pyrite or quartz) is not strictly equivalent to that mineral, but rather is is a particle with a chemical composition similar to that mineral. Assuming that the particles are spheres, the pixel area of the particles is used to calculate a diameter. The assumption that the particles are spherical can be justified for fly ashes, but it is critical for coal minerals and other materials with more irregular particle shapes. The diameter is used to group the particles into one of 8 size groups (1-2 μm, 2-4 μm, 4-8 μm, 8-16 μm, 16-32 μm, 32-64 μm, 64-125 μm, 125-250 μm).

The area analyzed at the high magnification (500x) with particles of 1-4 μm is much smaller than the area analyzed at medium (100x) and low (25x) magnification. To give the small particles a statistical correct representation in the analyses the area analyzed at high and medium magnifications are normalized to cover as large an area as analyzed by the low magnification. The total area analyzed at medium magnification (100x) is corrected with the equation:

$$F1*N1 / F2*N2,$$

and the high magnification (500x) is corrected with the equation:

$$F1*N1 / F3*N3,$$

where F1, F2 and F3 is the frame size (μm^2) at 25x, 100x and 500x, and N1, N2, and N3 are the number of frames analyzed at 25x, 100x and 500x. The correction factor for the particles analyzed at medium magnification is:

$$\text{area correction} = \frac{(\text{frame length}(25x) - \text{guard region})^2 * \text{frames}(25x)}{(\text{frame length}(100x) - \text{guard region})^2 * \text{frames}(100x)}$$

The correction factor for the particles analyzed at high magnification is:

$$\text{area correction} = \frac{(\text{frame length}(25x) - \text{guard region})^2 * \text{frames}(25x)}{(\text{frame length}(500x) - \text{guard region})^2 * \text{frames}(500x)}$$

The guard region is a region set at the border of each frame to avoid analyzing particles, which are only partly represented in the image. The guard region is set to be equal to half the size of the maximum particle size analyzed at each magnification (i.e. 25x: 125 μm; 100x: 16 μm; 500x: 2 μm). In practice each particle analyzed at 100x and 500x is multiplied by the area correction factor, which makes it possible to calculate the "weight percentage" of each category. After the magnification correction an area weight of each particle is calculated by multiplying the area of each particle with the density of the category. Finally, the weight percentage of each corrected particle is determined by dividing the area weight by the total sum of the area weight percentages for all the particles.

In many cases it is convenient to give the concentration of an element on an oxide basis. Thus, each element is multiplied by a gravimetric conversion factor, which are Na (1.3480), Mg (1.6579), Al (1.8895), Si (2.1392), P (2.2914), S (2.4969), Cl (2.5797), K (1.2046), Ca (1.3992), Ti (1.6681), Cr (1.4615), Fe (1.4297), Ni (1.2726), and Cu (1.1259). Finally, these data are corrected to a total oxide sum of 100%. It has to be underlined that the original chemical compositions of the particles were <u>not</u> element concentrations, but percent of counts, thus, the output after the conversion to oxide basis are also <u>semi-quantitative</u>.

The output from the data reduction is combined in 5 data sheets (see Appendix A):

1) *Summary* - shows the main results of the analyses included in the four following sheets
2) *Weight percentages on a mineral basis* - shows the weight percentage on a mineral basis of each category in the 8 size ranges and in total.
3) *Number of particles analyzed in each size range* - shows the number of analyzed particles in each category and in total.

4) *Average composition of the categories* - shows a semi-quantitative average chemical composition of the categories in each size range.
5) *Average composition of the size ranges* - shows a semi-quantitative chemical composition of each size range and the bulk chemical composition.

In addition to the data sheets, varous graphical methods such as ternary diagrams, may be used to illustrate the chemical distribution of the particles present in the sample (Figure 3.6). The ternary diagrams shows the relative weight percentages present in the sample with the composition indicated by the location of the column.

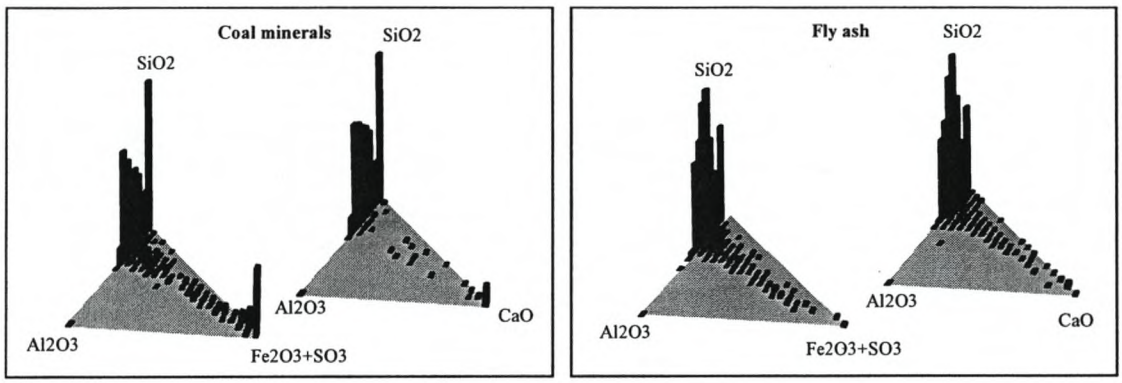

Figure 3.6. Fe_2O_3+SO_3-Al_2O_3-SiO_2 and CaO-Al_2O_3-SiO_2 ternary diagram.

On the ternary diagrams dominant minerals like quartz, clay, calcite and pyrite can be identified as peaks. The ternary diagrams also reveal information on the association between various minerals. If two minerals are connected the binary image will detect them as one particles and they will be analyzed as one particle and have a chemical composition which is a mix of the two minerals. Thus, a high concentration of particles with compositions between the mineral end-members indicate that these minerals are closely associated in the coal particles.

The grain size distribution of the minerals can be illustrated on a log grain size - cumulative weight percentage diagram (Figure 3.7). On the grain size diagram the maximum, the minimum and the median grain size can be determined.

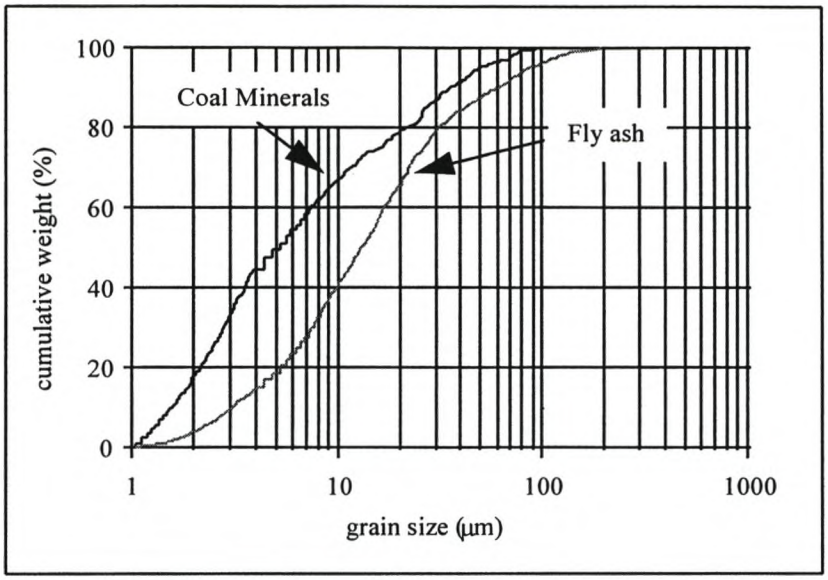

Figure 3.7. Log grain size(μm) - cumulative weight percentage diagram for minerals in coal and fly ash determined by CCSEM.

4. Scanning Electron Microscopy Point Counting (SEMPC)

The Scanning Electron Microscopy Point Counting (SEMPC) technique was developed on the SEM equipment at GEUS in order to achieve chemical data from highly inhomogenous materials, such as ash deposits, but it is highly useful on many other materials. The SEMPC technique can be used to quantify the various phases present in ashes and deposits. The technique is based on the widely used technique in light microscopy, point counting, but here the light microscope is substituted with a scanning electron microscope. Representative areas of a sample are chosen and the SEM is set to perform EDX analyses in a grid pattern in each of the areas (Figure 4.1). The number of points performed within an area may include as few as 25 points (5 x 5) up to as many as 10000 (100 x 100), depending on the magnification and the time available to perform the analyses.

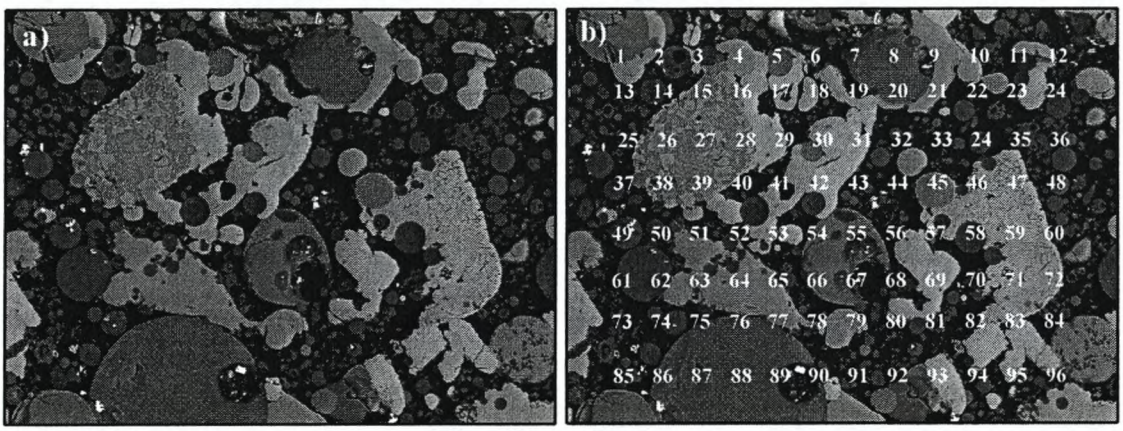

Figure 4.1. a) BSE image of ash deposit. b) distribution of point within a 12 x 8 points grid.

Within each point a preliminary EDX spectrum is collected for two seconds. If the total number of counts is below a certain threshold (operator selected) the beam is moved to the next point in the grid. If the total number of counts is above the threshold a spectrum is collected for 20 seconds. The counting time may, off course, be changed to shorter or longer time, dependent on the material and the desired analytical accuracy. The EDX spectrum for each of the accepted points is quantified and ZAF corrected to yield a quantitative chemical composition. Unlike the CCSEM method the SEMPC technique provides quantitative chemical compositions of each analyzed point. The chemical data are collected in a data file containing the point number and the elemental and oxide composition (Si, Al, Fe, Ca, Mg, Na, K, Mn, P, S, Cr, Ti, V) of each point. The chemical composition of the points is used to group each point into one of 32 chemical categories (Table 4.1). The categories used at GEUS are based on work done at the Energy and Environmental Research Center at University of North Dakota (Zygardlicke & Steadman, 1990; Jones et al., 1992). Based on the SEMPC data weight percentages of the categories / phases can be determined. Additionally, the bulk-chemistry of the deposits may be calculated. Appendix B includes an example on the results of a SEMPC analyses.

quartz: Si >=77
iron oxide: Fe >=72
calcium oxide: Ca > 74
rutile: Ti > 80
alumina: Al > 77
magnesium oxide: Mg > 74
dolomite: Mg > 5, Ca > Mg, S < 1, Mg+Ca > 74
mullite: Si > 3, Al > 5, Ca < 2, Fe < Si, Si+Fe+Al > 74, (0.21*Al) < Si, Si < (0.47*Al)
kaolinite-derived: Na <=5, K <=5, Ca <=5, Fe <=5, Al+Si > 80, (0.73*Al) < Si, Si < (1.5*Al)
montmorillonite-derived: Na<=5, K<=5, Ca <=5, Fe <=5, Al+Si > 80, (1.5*Al)< Si, Si< (2.5*Al)
illite-derived Na <=5, Al >=15, Si > 20, K > 5, K+Al+Si >=80, Ca <=5, Fe <=5
nepheline: Na > 4, Si > 4, Al > 4, Si+Na+Al > 74, (Na*0.97) < Si, Si < (1.58*Na), (Na*0.94) < Al, Al < (1.52*Na), (Al*0.83) < Si, Si < (1.35*Al)
pyrite: Fe > 5, S > 5, Fe+S > 74, (Fe*0.42) < S, S < (0.66*Fe)
pyrrhotite: Fe > 5, S > 5, Fe+S > 74, (Fe*0.66) < S, S < (1*Fe)
iron sulfate: Fe > 5, S > 5, Fe+S > 74, (Fe*1) < S, S < (1.7*Fe)
calcium sulfate: Ca+S > 84, (0.64*Ca) < S, S < (0.96*Ca)
sodium sulfate: Na > 5, S > 5, Fe+S > 74, (Na*1.3) < S, S < (1.58*Na)
Fe-Ca sulfat: S > 25, Fe > 25, Ca > 25, Ca+S+Fe > 80
apatite: P <=3, Ca >=4, Ca+P > 77, (1.55*P) < Ca, (2.58*P) < Ca
spinel: Al > 1, Ca < 2, Si < 2, Mg+Al+Fe > 91
ankerite: Mg < Fe, Si < 5, S < 5, Ca > 20, Fe > 20, Ca+Mg+Fe+Mn > 80
Fe-Al silicate: Na <=5, Al >=15, Si > 20, S <=5, K <=5, Ca <=5, Fe > 5, Fe+Al+Si >=80
Ca-Al silicate: Na <=5, Al >=15, Si > 20, S <=5, K <=5, Ca >=5, Ca+Al+Si >=80, Fe <=5
Na-Al silicate: Na >=5, Al >=15, Si > 20, Na+Al+Si >=80, S <=5, K <=5, Ca <=5, Fe <=5
aluminosilicate: Na <=5, Al > 20, Si > 20, Si+Al >=80, K <=5, Ca <=5, Fe <=5
mixed silicate: Na < 10, Al > 20, Si > 20, S <=5, K < 10, Ca < 10, Fe < 10, Na+Al+Si+K+Ca+Fe >80
Fe silicate: Na <=5, Al <=5, Si < 20, S <=5, K <=5, Ca <=5, Fe > 10, Fe+Si >=80
Ca silicate: Na <=5, Al <=5, Si > 20, S <=5, K <=5, Ca > 10, Ca+Si >=80, Fe <=5
Ca aluminate: Al > 5, Ca > 6, Si < Al, Al+Ca > 77, (Al*1.48) < Ca, Ca < 2.96*Al
Fe-Cr oxide: Fe+Cr > 70, Fe > 35, S < 15
Cr-Fe oxide: Fe+Cr > 70, Fe < 35, S < 15
KCl: K >=30, Cl >=30, K+Cl >=80
unknown: all non-categorized

Table 4.1. Chemical classification system for SEMPC data.

As for the CCSEM analyses various graphical illustrations may be used present the chemical data (Figure 4.2). The histograms are useful for illustrating the mass fraction of particles with a specified content of an element (e.g.Fe_2O_3 or CaO). The histograms may be viewed as having been constructed by determining the iron content in strips cut from the ternary diagrams along lines parallel to the SiO_2-Al_2O_3 side.

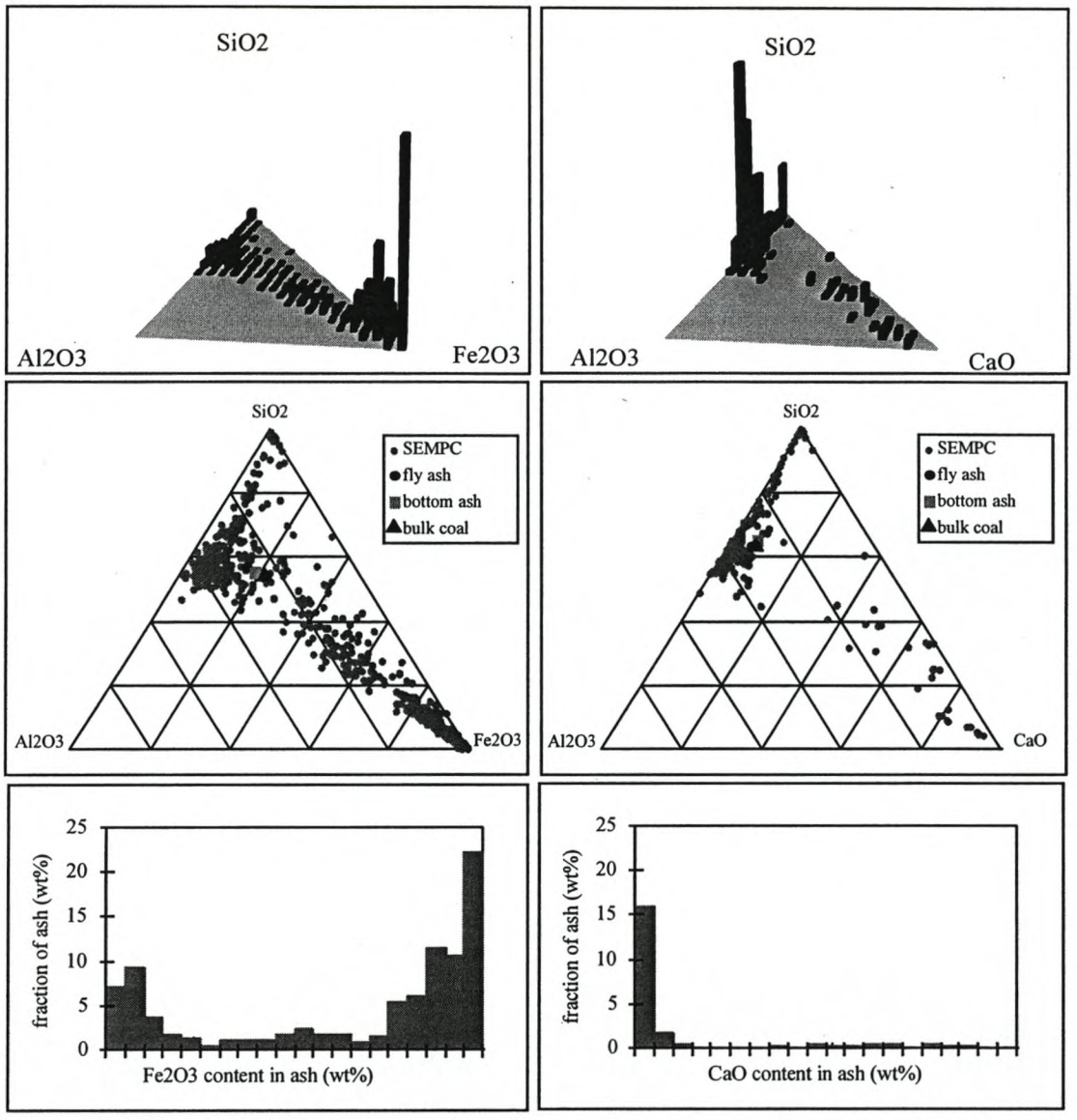

Figure 4.2. Fe_2O_3-SiO_2-Al_2O_3 and SiO_2-Al_2O_3-CaO ternary diagrams, and Fe_2O_3 and CaO histograms for SEMPC analysis and bulk-chemical (ICP-AES) analyses of a boiler deposit. The heights of the columns of the 3D ternary diagrams show the relative weight percentages present in the sample with the composition indicated by the location of the column. Only particles with a total sum > 80% for the corner elements are shown.

Image analyses of the areas used for SEMPC analyses may be used to determine the porosity of the deposits or material. The porosity is determined as the area percentage covered by the embedding material (pores) divided by the total area of the image field.

5. References

Goldstein J.I., Newbury D.E., Echlin P., Joy D.C., Romig A.D., Lyman, C.E., Fiori, C. & Lifshin E. (1992) Scanning electron microscopy and x-ray analysis. A text for biologists, materials scientists. and geologists. Second edition. Plenum Press. New York and London.

Huggins F.E., Kosmack D.A., Huffman G.P. & Lee R.J. (1980) Coal mineralogy by SEM image analysis. Scanning Electron Microscopy. 1. (p 531-540)

Jones M.L., Kalmanovitch D.P., Steadman E.N., Zygarlicke J & S.A. Benson (1992) Application of SEM techniques to the characterization of coal and coal ash products. In Advances in coal spectroscopy. Edited by Meuzelaar H.L.C. Plenum. (p. 1-27).

Lee R.J., Huggins F.E. & Huffman G.P. (1978) Correlated Mossbauer-SEM studies of coal mineralogy. Scanning Electron Microscopy. Vol. 1 (p. 561-568).

Mortimer C.E. (1983) Chemistry. Fifth Edition. Wadswoth Publishing Company.

Sears F.W., Zemansky M.W. & Young H.D. (1981) University physics. Sixth Edition. Addison-Wesley Publishing Company.

Skorupska N.M. & Carpenter A.M. (1993) Computer controlled scanning electron microscopy of minerals in coal. IEA Coal Research. Perspectives (p.1-21).

Southworth H.N. (1975) Scanning electron microscopy and microanalysis. In Physicochemical methods of mineral analysis. Edited by A.W. Nicol. Plenum Press.(p. 421-449).

Zygardlicke C.J. & Steadman E.N. (1990) Advanced SEM techniques to characterize coal minerals. Scanning Microscopy. Vol 4. No. 3. (p. 579-590).

APPENDIX A

Results of a CCSEM analyses of a pulverized coal

Summary: El Cerrejon coal

Catagory	Weight percent	Number of particles
alumina	0.09	1
aluminosilicate	3.82	48
ankerite	0.02	1
apatite	1.40	16
Ca silicate	0.09	3
Ca-Al silicate	0.31	7
Ca-Al-P	0.04	1
Ca-rich	0.08	3
Ca-Si-rich	0.18	2
calcite	1.01	14
clay-pyrite	3.77	33
dolomite	1.36	18
Fe silicate	0.12	3
Fe-Al silicate	2.37	56
Fe-Cr oxid	0.93	12
gypsum	2.96	37
gypsum/Al silicate	0.27	11
gypsum/rutile	0.10	2
illite	25.72	499
iron oxide	0.93	5
kaolinite	7.53	134
mixed silicate	1.17	30
montmorillonite	5.06	122
oxi. pyrrhotite	0.35	2
pyrite	6.64	73
pyrrhotite	0.30	4
quartz	19.34	360
rutile	0.14	4
Si-rich	3.74	77
unknown	10.16	162
Grand Total:	**100.00**	**1740**

Bulk Chemistry based on CCSEM analysis

SiO2	63.72
Al2O3	17.56
Fe2O3	3.76
CaO	4.36
MgO	0.39
Na2O	0.00
K2O	2.41
P2O5	0.59
SO3	6.42
Cr2O3	0.05
TiO2	0.65
Cl2O7	0.08

Weight percent on a mineral basis - El Cerrejon coal

	1-2 um	2-4 um	4-8 um	8-16 um	16-32 um	32-64 um	64-125 um	125-250 um	Total
alumina				0.09					0.09
aluminosilicate	0.11		0.39	0.80	1.09	0.76	0.67		3.82
ankerite			0.02						0.02
apatite	0.16	1.00	0.12	0.12					1.40
Ca silicate			0.03	0.06					0.09
Ca-Al silicate	0.02	0.07	0.05	0.17					0.31
Ca-Al-P	0.04								0.04
Ca-rich	0.06		0.02						0.08
Ca-Si-rich			0.03			0.16			0.18
calcite	0.02	0.25	0.03	0.18		0.54			1.01
clay-pyrite	0.06	0.32	0.20	0.66	0.52	1.07	0.94		3.77
dolomite	0.02		0.09	0.29	0.26	0.22	0.48		1.36
Fe silicate	0.09		0.04						0.12
Fe-Al silicate	0.28	0.51	0.64	0.59		0.14	0.21		2.37
Fe-Cr oxid	0.10	0.37	0.26	0.21					0.93
gypsum		0.22	0.32	0.52	1.37	0.53			2.96
gypsum/Al silicate			0.17	0.10					0.27
gypsum/rutile	0.10								0.10
illite	1.96	4.95	5.21	5.62	4.96	2.68	0.35		25.72
iron oxide	0.11	0.78	0.04						0.93
kaolinite	0.27	0.90	1.48	1.04	1.91	1.16	0.76		7.53
mixed silicate	0.25	0.34	0.27	0.19		0.12			1.17
montmorillonite	0.53	2.10	1.16	0.29	0.37	0.45	0.16		5.06
oxi. pyrrhotite				0.35					0.35
pyrite	0.92	0.31	1.49	2.34	1.00	0.59			6.64
pyrrhotite	0.09		0.04			0.16			0.30
quartz	1.59	3.37	3.80	3.77	2.91	2.18	1.72		19.34
rutile	0.11		0.03						0.14
Si-rich	0.04	0.08	1.00	1.14	1.09	0.38			3.74
unknown	0.66	1.45	1.32	1.76	1.39	1.70	1.18	0.69	10.16
	7.58	**17.00**	**18.23**	**20.30**	**16.86**	**12.86**	**6.47**	**0.69**	**100.00**

Number of particles analyzed in each size range - El Cerrejon coal

	1-2 um	2-4 um	4-8 um	8-16 um	16-32 um	32-64 um	64-125 um	125-250 um	Total
alumina				1					1
aluminosilicate	4		19	10	3	10	2		48
ankerite			1						1
apatite	3	7	5	1					16
Ca silicate			2	1					3
Ca-Al silicate	1	1	3	2					7
Ca-Al-P	1								1
Ca-rich	2		1						3
Ca-Si-rich			1			1			2
calcite	1	3	2	2		6			14
clay-pyrite	1	2	9	6	2	10	3		33
dolomite	1		5	5	1	4	2		18
Fe silicate	2		1						3
Fe-Al silicate	8	3	34	8		2	1		56
Fe-Cr oxid	2	1	7	2					12
gypsum		1	14	7	5	10			37
gypsum/Al silicate			9	2					11
gypsum/rutile	2								2
illite	58	40	267	76	18	38	2		499
iron oxide	2	2	1						5
kaolinite	8	7	79	17	7	14	2		134
mixed silicate	8	3	14	3		2			30
montmorillonite	20	19	68	6	2	6	1		122
oxi. pyrrhotite				2					2
pyrite	17	2	36	11	3	4			73
pyrrhotite	1		1			2			4
quartz	50	25	185	53	11	30	6		360
rutile	3		1						4
Si-rich	2	1	50	15	3	6			77
unknown	23	11	70	26	5	21	5	1	162
	220	**128**	**885**	**256**	**60**	**166**	**24**	**1**	**1740**

Average composition of categories - El Cerrejon coal

	Si	Al	Fe	Ca	Mg	Na	K	Ti	P	S	Cl	Cr	Ni	Cu
alumina	0.00	100.00	0.00	0.00	0.00	0.00	0.00	0.00	0.00	0.00	0.00	0.00	0.00	0.00
aluminosilic	74.54	24.47	0.00	0.00	0.00	0.00	0.68	0.00	0.00	0.17	0.15	0.00	0.00	0.00
ankerite	0.00	0.00	65.98	24.62	9.40	0.00	0.00	0.00	0.00	0.00	0.00	0.00	0.00	0.00
apatite	1.10	0.57	0.00	71.34	0.00	0.00	0.00	0.00	26.99	0.00	0.00	0.00	0.00	0.00
Ca silicate	43.46	3.03	0.00	51.93	0.00	0.00	0.00	0.00	0.00	1.59	0.00	0.00	0.00	0.00
Ca-Al silicat	55.08	25.31	0.00	17.53	0.00	0.00	0.00	0.00	2.07	0.00	0.00	0.00	0.00	0.00
Ca-Al-P	3.92	36.79	0.00	12.32	0.00	0.00	5.15	8.86	32.95	0.00	0.00	0.00	0.00	0.00
Ca-rich	6.63	0.00	0.00	93.37	0.00	0.00	0.00	0.00	0.00	0.00	0.00	0.00	0.00	0.00
Ca-Si-rich	39.81	10.59	0.00	46.35	3.27	0.00	0.00	0.00	0.00	0.00	0.00	0.00	0.00	0.00
calcite	1.19	0.31	0.00	98.50	0.00	0.00	0.00	0.00	0.00	0.00	0.00	0.00	0.00	0.00
clay-pyrite	32.37	10.50	17.16	0.35	0.00	0.00	0.90	0.00	0.00	38.72	0.00	0.00	0.00	0.00
dolomite	1.06	0.00	4.56	82.14	11.39	0.00	0.00	0.00	0.00	0.48	0.38	0.00	0.00	0.00
Fe silicate	12.37	0.00	83.29	0.00	0.00	0.00	0.00	2.00	0.00	0.00	2.33	0.00	0.00	0.00
Fe-Al silicat	49.99	24.35	20.72	0.09	3.73	0.00	0.76	0.09	0.00	0.15	0.11	0.00	0.00	0.00
Fe-Cr oxid	4.56	1.38	75.79	11.36	5.83	0.00	0.50	0.00	0.00	0.00	0.00	0.58	0.00	0.00
gypsum	1.18	0.00	0.54	56.71	0.00	0.00	0.00	0.00	0.00	41.56	0.00	0.00	0.00	0.00
gypsum/Al si	30.05	13.21	3.78	31.76	0.83	0.00	3.36	0.00	0.00	16.44	0.56	0.00	0.00	0.00
gypsum/rutil	0.00	0.00	0.00	7.78	0.00	0.00	0.00	54.82	0.00	37.39	0.00	0.00	0.00	0.00
illite	61.24	26.94	0.27	0.11	0.04	0.00	10.72	0.27	0.00	0.31	0.04	0.05	0.02	0.00
iron oxide	4.77	0.00	87.55	3.42	0.00	0.00	1.82	0.00	0.00	0.00	1.38	1.05	0.00	0.00
kaolinite	57.68	41.89	0.00	0.00	0.00	0.00	0.06	0.06	0.13	0.09	0.00	0.03	0.06	0.00
mixed silicat	57.43	27.17	5.31	2.16	0.16	0.00	6.90	0.00	0.00	0.45	0.00	0.42	0.00	0.00
montmorillo	62.68	36.30	0.04	0.00	0.00	0.00	0.38	0.21	0.00	0.23	0.08	0.09	0.00	0.00
oxi. pyrrhoti	3.45	0.00	86.86	3.80	0.00	0.00	0.00	0.00	0.00	5.90	0.00	0.00	0.00	0.00
pyrite	2.32	0.53	30.01	0.05	0.00	0.00	0.00	0.05	0.00	66.97	0.00	0.07	0.00	0.00
pyrrhotite	5.34	2.16	45.27	0.00	0.00	0.00	0.00	0.00	0.00	47.22	0.00	0.00	0.00	0.00
quartz	97.56	2.02	0.04	0.04	0.00	0.00	0.15	0.09	0.00	0.08	0.00	0.00	0.00	0.00
rutile	1.81	1.24	1.00	0.00	0.00	0.00	0.00	94.87	0.00	0.00	0.00	1.09	0.00	0.00
Si-rich	84.17	14.13	0.00	0.00	0.00	0.00	1.64	0.06	0.00	0.00	0.00	0.00	0.00	0.00
unknown	47.03	16.36	12.15	7.78	0.79	0.00	5.10	3.30	1.72	5.22	0.18	0.20	0.15	0.02

Average composition of the size ranges - El Cerrejon coal

	Si	Al	Fe	Ca	Mg	Na	K	Ti	P	S	Cl	Cr	Ni	Cu
1) 1-2 um	56.65	18.25	6.33	3.66	0.25	0.00	3.86	2.83	1.23	6.77	0.07	0.10	0.00	0.00
2) 2-4 um	57.08	19.60	4.79	8.76	0.29	0.00	4.11	0.36	1.69	3.12	0.12	0.05	0.03	0.00
3) 4-8 um	62.77	19.61	4.37	3.37	0.41	0.00	4.21	0.48	0.20	4.39	0.06	0.08	0.04	0.00
4) 8-16 um	60.61	16.93	5.42	6.42	0.45	0.00	3.68	0.30	0.43	5.76	0.00	0.00	0.00	0.00
5) 16-32 um	59.26	17.86	3.97	6.10	0.22	0.00	3.24	0.81	0.00	8.54	0.00	0.00	0.00	0.00
6) 32-64 um	58.47	15.47	4.51	9.79	0.36	0.00	2.98	0.21	0.00	8.09	0.08	0.04	0.00	0.00
7) 64-125 um	63.29	14.60	4.76	7.51	0.85	0.00	2.07	0.00	0.00	6.92	0.00	0.00	0.00	0.00
8) 125-250 um	78.21	16.61	0.00	0.00	0.00	0.00	0.00	0.00	0.00	5.18	0.00	0.00	0.00	0.00
	59.90	**17.79**	**4.75**	**6.46**	**0.37**	**0.00**	**3.57**	**0.59**	**0.50**	**5.98**	**0.05**	**0.04**	**0.01**	**0.00**

APPENDIX B

Results of a SEMPC analyses of slag deposit

NVV2-16 (upstream deposit)

07-Jan-97

Catagory	Weight percent	Number of particles
aluminosilicate	0.45	4
ankerite	0.12	1
Ca-Al silicate	1.90	17
calcium oxide	0.47	4
Fe silicate	0.19	1
Fe-Al silicate	15.26	129
Fe-Cr oxide	1.86	9
illite-derived	0.91	8
iron oxide	38.97	174
kaolinite-derived	4.03	36
mixed silicate	2.58	23
montmorillonite-derived	0.63	6
Na-Al silicate	0.11	1
pyrite	3.80	18
pyrrhotite	1.37	12
quartz	2.24	20
unknown	25.10	220
Grand Total:	**100.00**	**683**

Bulk-chemical composition of the deposit

SiO2	31.33
Al2O3	15.59
Fe2O3	35.56
CaO	6.80
MgO	0.78
Na2O	1.46
K2O	0.90
MnO	0.27
P2O5	1.19
SO3	4.52
Cr2O3	0.28
TiO2	0.94
Cl	0.27

Chemical composition - NVV2-16 (upstream deposit)

07-Jan-97

catagory	SiO2	Al2O3	Fe2O3	CaO	MgO	Na2O	K2O	MnO	P2O5	SO3	Cr2O3	TiO2	Cl	percent
aluminosilicate	71.19	19.46	1.87	0.58	0.25	1.67	2.05	0.27	0.12	0.29	0.06	1.55	0.38	0.45
ankerite	7.22	3.95	63.68	20.83	0.36	1.32	0.09	0.18	0.44	0.58	0.28	0.74	0.32	0.12
Ca-Al silicate	40.64	24.06	2.37	24.22	2.07	0.66	0.54	0.37	2.69	0.54	0.24	1.45	0.09	1.90
calcium oxide	3.75	2.29	5.42	84.25	1.09	0.17	0.22	0.67	0.37	0.57	0.22	0.57	0.22	0.47
Fe silicate	25.15	5.87	60.44	3.08	0.49	2.25	0.79	0.00	0.42	0.68	0.18	0.64	0.00	0.19
Fe-Al silicate	49.32	29.24	12.19	1.74	0.76	1.83	1.86	0.29	0.34	0.37	0.19	1.34	0.42	15.26
Fe-Cr oxide	14.29	8.38	65.85	6.08	0.46	1.71	0.20	0.16	0.14	2.06	0.03	0.53	0.04	1.86
illite-derived	59.86	29.06	2.28	0.45	0.74	1.49	3.52	0.18	0.26	0.18	0.17	1.36	0.42	0.91
iron oxide	6.47	3.43	83.48	0.80	0.38	1.73	0.14	0.31	0.13	2.16	0.46	0.29	0.10	38.97
kaolinite-derive	51.58	38.90	2.49	0.84	0.31	1.41	2.02	0.16	0.13	0.23	0.21	1.31	0.33	4.03
mixed silicate	53.41	29.87	4.66	3.44	0.80	2.24	2.37	0.42	0.27	0.58	0.19	1.31	0.32	2.58
montmorillonite	61.06	28.34	2.42	1.01	0.61	1.53	2.32	0.57	0.19	0.14	0.37	0.99	0.43	0.63
Na-Al silicate	61.45	26.45	1.32	1.27	0.07	6.63	2.22	0.00	0.00	0.52	0.00	0.00	0.00	0.11
pyrite	3.56	1.94	47.01	0.37	0.24	1.04	0.12	0.14	0.21	44.74	0.11	0.21	0.23	3.80
pyrrhotite	1.12	0.63	43.74	0.24	0.20	0.70	0.05	0.09	0.15	52.73	0.05	0.02	0.17	1.37
quartz	90.21	3.18	2.61	0.43	0.12	0.64	0.85	0.29	0.08	0.56	0.14	0.49	0.27	2.24
unknown	31.28	13.98	26.15	15.07	1.24	1.16	0.64	0.24	3.05	5.27	0.27	1.23	0.33	25.10